Dual-axis tilting rotor quad-plane design, simulation, flight and performance comparison with a conventional quad-plane design

Mancinelli, Alessandro; Smeur, Ewoud J.J.; Remes, Bart; Croon, Guido De

DOI
10.1109/ICUAS54217.2022.9836063

Publication date
2022

Document Version
Final published version

Published in
2022 International Conference on Unmanned Aircraft Systems, ICUAS 2022

2022 International Conference on Unmanned Aircraft Systems (ICUAS)
Dubrovnik, Croatia. June 21-24, 2022

2022 International Conference on Unmanned Aircraft Systems (ICUAS) | 978-1-6654-0593-5/22/$31.00 ©2022 IEEE | DOI: 10.1109/ICUAS54217.2022.9836063

Dual-axis tilting rotor quad-plane design, simulation, flight and performance comparison with a conventional quad-plane design

1st Alessandro Mancinelli
Department of Control and Simulation
Delft University of Technology
Delft, The Netherlands
A.Mancinelli@tudelft.nl

2nd Ewoud J.J. Smeur
Department of Control and Simulation
Delft University of Technology
Delft, The Netherlands
E.J.J.Smeur@tudelft.nl

3rd Bart Remes
Department of Control and Simulation
Delft University of Technology
Delft, The Netherlands
B.D.W.Remes@tudelft.nl

4th Guido de Croon
Department of Control and Simulation
Delft University of Technology
Delft, The Netherlands
G.C.H.E.Decroon@tudelft.nl

***Abstract*—In the last few decades, the UAV research has been focusing on hybrid vehicles with Vertical Takeoff and Landing (VTOL) capabilities. Opposed to copters, hybrid vehicles are highly influenced by wind disturbances. This paper presents a novel quad-plane design that uses four dual-axis tilting rotors to enhance the wind rejection capability of a conventional quad-plane vehicle. After the non-linear mathematical model derivation and the actuator identification, the performance of the vehicle is addressed and compared to a conventional quad-plane in simulation, showing a factor 3.4 improvement in linear acceleration reaction time and a reduction of the gust induced displacement of 80%. Free-flight wind tunnel experiments confirmed the simulation outcome and extended the vehicle wind rejection capabilities behavior also to the lateral gust scenario.**

***Index Terms*—UAV, VTOL, Tilting rotors, Quad-plane, Wind disturbance rejection capability, Hybrid MAVs**

I. Introduction

In the last twenty years, a boom in the Unmanned Aerial Vehicle industry has been experienced all over the world. In particular, the development has been focusing on VTOL UAVs. The development of brushless motors and MEMS, together with a huge leap in the battery and the microprocessor technology, allowed the development of small and cheap UAVs capable of controlled vertical takeoff and landing without the necessity of a complex swash plate system typical of rotary wing vehicles. Of particular interest are the so called 'hybrid' vehicles, able to combine the cruise efficiency of conventional fixed wing planes with hovering capability. One kind of hybrid VTOL vehicle is the quad-plane: a conventional fixed wing UAV equipped with four fixed rotors in a multi-copter configuration, allowing the UAV to takeoff and land vertically. An example of such a quad-plane can be found in [1]. Once in hovering flight, the quad-plane can transition to forward flight by gradually increasing the thrust of the forward motor and switching off the vertical lifting rotors.

Another design of the quad-plane, presented in 2012 by Gerardo Ramon Flores et al. [2], was able to make use of the same motors for both the hovering and the forward configuration. This was possible thanks to a mechanism able to synchronously tilt all the rotors of 90 degrees. An Cheng et al. [3] presented a quad-plane with only three rotors, two of which are independently tiltable. This feature improves the yaw authority of the vehicle in the hovering phase, relying on differential tilt rather than differential thrust.

However, as almost every VTOL platform with a non negligible wing surface, quad-plane designs are highly influenced by wind disturbances. In previous work, Hang Zhang et al. [4] successfully analyzed the steady wind rejection capabilities of such vehicles in detail. Unfortunately, the analysis is limited to the static rejection capability and does not consider the vehicle dynamics. Due to their limited degrees of freedom, conventional quad-plane platforms tend to reject the wind by changing the attitude. Because the attitude dynamics of such vehicles are typically slow, the disturbance rejection capability is also slow.

Another relevant limitation related to lacking full 6 degree of freedom authority, is the impossibility of independently achieving any desired rotation and translation in the 3D space. This limitation is particularly penalizing when a precision landing is attempted on a moving and tilting platform such as a ship at sea.

To address the maneuvering limitations of quadrotors, Ali Bin Junaid et al. [5] designed a quad-copter with dual-axis tilting rotors and full 6 DOF authority. Through various flight

Project founded by the Europees Fonds voor Regionale Ontwikkeling (EFRO)

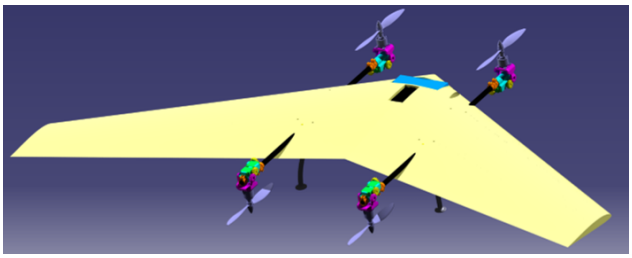

Fig. 1: Render of the proposed vehicle, isometric view.

tests in constrained space achieving complex trajectory they proved the effectiveness of a tilting rotor system to enhance the quad-copter agility and mobility.

The contribution of this work is the extension of this concept to a quad-plane vehicle and the evaluation of the wind rejection capabilities and overall performance of the resulting vehicle.

We propose a novel quad-plane design consisting of a flying wing structure propelled with only four motors used for both the hovering and the forward flight condition. The special aspect of the rotors is their double axis tilting capability achieved thanks to two servomotors coupled with a specially developed gear mechanism. This gives the vehicle independent control over all 6 degrees of freedom. It is therefore possible to directly and independently achieve any combination of translation and rotation, leading to reactive and effective wind disturbance rejection.

The paper is organized as follows; In Section II the novel vehicle design is presented. In Section III, the mathematical model of the UAV is derived. In Section IV, the actuators are identified and modeled through several tests. In Section V, the results of the simulations are analyzed. In Section VI, the results of a flight test campaign conducted on the UAV in the wind tunnel are commented. Finally, in Section VII some conclusions are drawn.

II. Vehicle Design

The vehicle design consists of a blended wing body structure propelled with four dual-axis independently tiltable rotors acting as vertical and forward propellers. A render of the proposed vehicle prototype in hovering configuration is shown in Fig.1 while a summary of the vehicle characteristics is reported in Table I.

A. Wing design

The airfoil used for the wing design is a TL54, a reflex airfoil specifically developed for flying wing applications. In particular, since this wing was designed from scratch, a non-viscous analysis using the open-source software XFLR5[1] was run in order to identify the aerodynamic properties and the aerodynamic center of the wing. The knowledge of the aerodynamic center was also used during the weight distribution of the vehicle, in such a way to achieve a static

[1]http://www.xflr5.tech/xflr5.htm

CG location	256mm from root L.E.
Takeoff mass	2.3 kg
Vehicle Inertia I_{xx} in Γ_b	0.1 $[kg \cdot m^2]$
Vehicle Inertia I_{yy} in Γ_b	0.15 $[kg \cdot m^2]$
Vehicle Inertia I_{zz} in Γ_b	0.25 $[kg \cdot m^2]$
Rotor Inertia I_{xx} in Γ_p	$1.3 \cdot 10^{-4}$ $[kg \cdot m^2]$
Rotor Inertia I_{yy} in Γ_p	$1.5 \cdot 10^{-4}$ $[kg \cdot m^2]$
Length l_1	185 $[mm]$
Length l_2	185 $[mm]$
Length l_3	376 $[mm]$
Length l_4	290 $[mm]$

TABLE I: Physical characteristics of the prototype vehicle, see Fig.4 and Fig.5 for the nomenclature.

Profile	TL54
Root chord length	45 cm
Tip chord length	21 cm
Mean aerodynamic chord	33.25 cm
Wing surface	0.57 m^2
Total wing-span	1.85 m
Twist angle tip	-5 deg
Dihedral angle	0 deg
Sweep angle	28.7 deg
Wing a.c.	288mm from root L.E.

TABLE II: Specs of the designed wing

stability margin of 9.6%. A picture of the analyzed wing is visible in Fig.2 while the wing specifications are reported in Table II. After being designed, the wing was cut from a block of foam using a Computerised Numerical Control (CNC) machine.

B. Tilting mechanism design

The tilting mechanism and the motor support were designed to be entirely 3D printed using a commercial Filament Deposition Material machine. As rotation transmission medium, a gearing system was preferred to a pull/push rod system to allow linear torque and rotational speed distribution between servo and rotor. Moreover, by adjusting the number of teeth it is possible to adjust the torque and speed ratio between the servo and the rotor system.
The properties of the gear system on the azimuth and

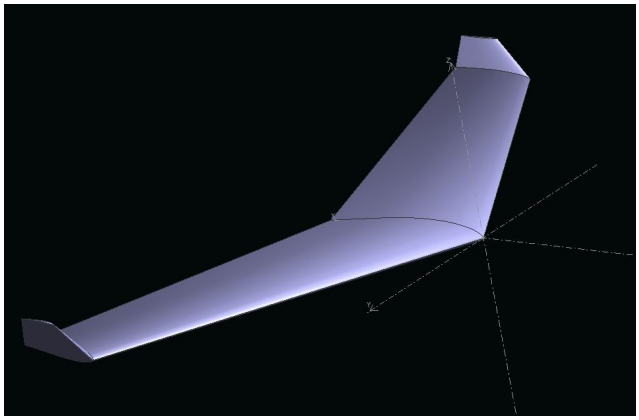

Fig. 2: Wing of the vehicle in XFLR5, isometric view.

Azimuth gear module	1.39 mm
N. teeth azimuth servo gear	14
N. teeth azimuth rotor gear	13
Elevation gear modulus	1.39 mm
N. teeth elevation servo gear	14
N. teeth elevation rotor gear	14
Max elevation angle	25 deg
Min elevation angle	-120 deg
Max elevation angle	45 deg
Min elevation angle	-45 deg

TABLE III: Specs of the designed tilting mechanism

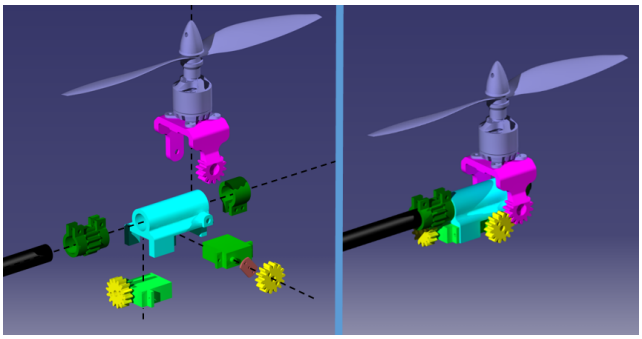

Fig. 3: Render of the tilting mechanism, exploded view on the left side and isometric view on the right side.

elevation tilting rotation are reported in Table III. As shown in Fig. 5, the azimuth rotor rotation is the rotation over the propeller x-axis (g_i angle) while the elevation rotor rotation is the rotation over the propeller y-axis (b_i angle). In Fig. 3, a render of an exploded and isometric view of the tilting mechanism is shown.

III. Mathematical Model

An accurate mathematical model of the vehicle was derived with the aim of simulating the UAV performance and to predict the servomotor load. Notice that under the condition of $b_i = 0$ and $g_i = 0$, the same mathematical model also applies to the conventional quad-plane dynamics in the hovering configuration.

The following assumptions were made during the mathematical model development:

- Aerodynamic interaction between wind and propeller is neglected.
- Thrust is always aligned with the local rotor vertical axis.
- The change of the body inertia due to the rotor tilting is negligible and x_b, y_b and z_b are vehicle principal axes.
- x_p, y_p and z_p are principal axes for the propeller, and the inertia terms I^p_{xx} and I^p_{yy} are negligible.
- The inertia tensor of the tilting mechanism in the propeller reference frame Γ_p is a diagonal matrix.

The rotors identification, rotating direction and disposition with reference to the CG are shown in Fig. 4.

A. Reference frames and transposing matrices

The reference frames used are the following:

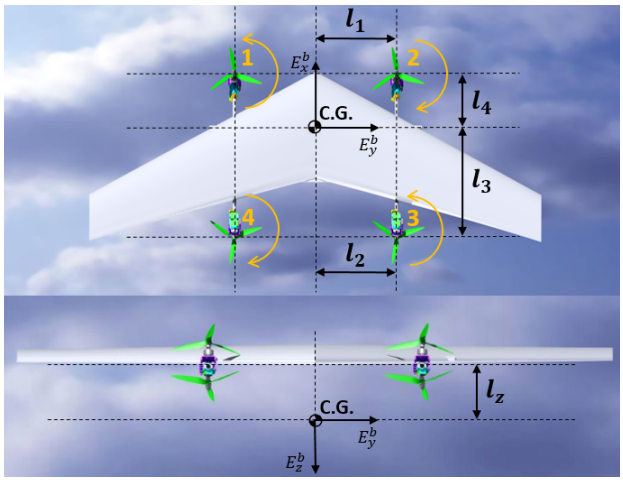

Fig. 4: Assumptions and notation for rotor identification, disposition and rotating direction

- Earth Frame Γ_e
  - Origin: fixed to the surface of the Earth
  - x_e axis: positive in the direction of north
  - y_e axis: positive in the direction of east
  - z_e axis: positive towards the center of the Earth
- Body Frame Γ_b
  - Origin: airplane center of gravity
  - x_b axis: positive out the nose of the aircraft in the plane of symmetry of the aircraft
  - y_b axis: perpendicular to x_b and z_b, positive out of the right wing
  - z_b axis: perpendicular to the x_b axis, in the plane of symmetry of the aircraft, positive below the aircraft
- Propeller Frame Γ^i_p
  - Origin: center of rotation of the rotor, rotor number identified by the index i
  - x_p axis: positive out the nose of the aircraft(in hovering configuration) and perpendicular to z_p
  - y_p axis: perpendicular to x_p and z_p, positive pointing the right direction of the aircraft in hovering configuration
  - z_p axis: aligned with the motor axis, pointing in the opposite thrust direction
- Wind Frame Γ_w
  - Origin: airplane center of gravity
  - x_w axis: positive in the direction of the velocity vector of the aircraft relative to the air
  - y_w axis: perpendicular to x_w and z_w, positive to the right
  - z_w axis: perpendicular to the x_w axis, in the plane of symmetry of the aircraft, positive below the aircraft

An overview of the main reference frames used in the model is also shown in Fig. 5. The transformation matrix from the frame Γ_b to Γ_e is derived from the classical ZYX composi-

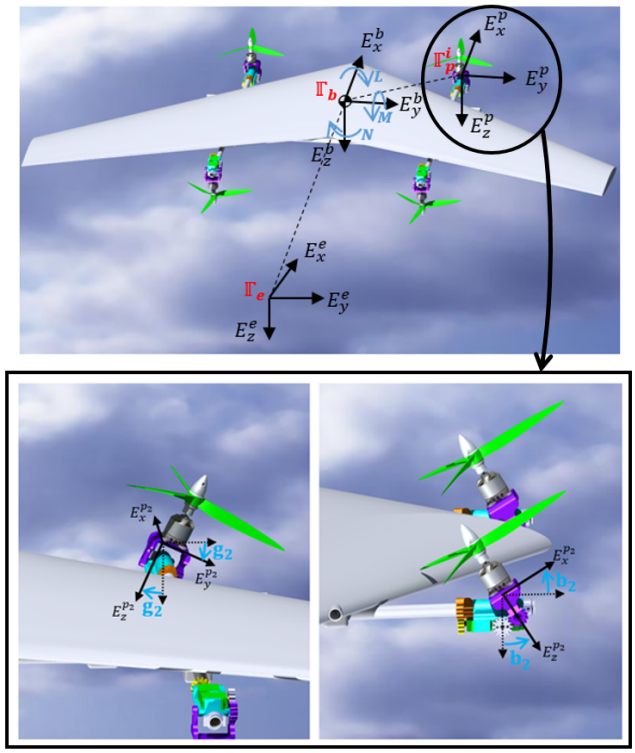

Fig. 5: Overview of the Earth, Body and Propeller frames.

tion of elementary Euler angles rotation and is reported as follows:

$$R_{eb} = \begin{bmatrix} c_\theta c_\psi & -c_\phi s_\psi + s_\phi s_\theta c_\psi & s_\phi s_\psi + c_\phi s_\theta c_\psi \\ c_\theta s_\psi & c_\phi c_\psi + s_\phi s_\theta s_\psi & -s_\phi c_\psi + c_\phi s_\theta s_\psi \\ -s_\theta & s_\phi c_\theta & c_\phi c_\theta \end{bmatrix} \quad (1)$$

Such that:

$$\begin{pmatrix} x_e \\ y_e \\ z_e \end{pmatrix} = R_{eb} \begin{pmatrix} x_b \\ y_b \\ z_b \end{pmatrix} \quad (2)$$

Notice that c and s are the abbreviation respectively of the cos and sin functions.

The transformation matrix from the frame Γ_p to Γ_b is derived from the YX composition of elementary rotation of the tilting angles g and b expressed in Fig. 5. The final matrix R_{bp} is the following:

$$R_{bp}^i = \begin{bmatrix} c(b^i) & 0 & s(b^i) \\ s(g^i)s(b^i) & c(g^i) & -s(g^i)c(b^i) \\ -c(g^i)s(b^i) & s(g^i) & c(g^i)c(b^i) \end{bmatrix} \quad (3)$$

Such that:

$$\begin{pmatrix} x_b \\ y_b \\ z_b \end{pmatrix} = R_{bp}^i \begin{pmatrix} x^p \\ y^p \\ z^p \end{pmatrix}_i \quad (4)$$

Where the suffix i indicates the rotor number. This specification is necessary since the rotors can tilt independently from each other.

Finally, the transformation matrix from the frame Γ_w to Γ_b is derived from the YZ composition of elementary rotation of the slide slip angle and the angle of attack. The final matrix R_{bw} is the following:

$$R_{bw} = \begin{bmatrix} c(\alpha)c(\beta) & -c(\alpha)s(\beta) & -s(\alpha) \\ s(\beta) & c(\beta) & 0 \\ s(\alpha)c(\beta) & -s(\alpha)s(\beta) & c(\alpha) \end{bmatrix} \quad (5)$$

Where α is the angle of attack and β is the sideslip angle.

B. Equations of motion

After having defined the frames and the rotational matrices, it is possible to analyze all the forces and moments acting on the vehicle with the aim of determining the equations of motion. Considering the assumptions given above, the equations of motion for the vehicle are the following:

$$\begin{cases} \ddot{P}_b = \frac{1}{m}\left(F_p + F_a^{wb}\right) + g\hat{z}_e \\ \dot{\omega} = I_b^{-1}\left(-\omega \times I_b\omega + M_p^T + M_p^D + M_p^I + \right. \\ \qquad \left. + M_r^p + M_a^{wb} + M_p^t + M_r^{tilt}\right) \end{cases} \quad (6)$$

Where $\ddot{P}_b$ are the linear acceleration in the earth reference frame and $\dot{\omega}$ are the derivative of the vehicle body rate.

Each term in equation (6) refers to a specific effect and can be analyzed in detail as follows:

- F_p : Forces produced by the propeller thrust rotated to the earth frame:

$$F_p = \sum_{i=1}^{N} R_{eb} R_{bp}^i \begin{pmatrix} 0 \\ 0 \\ -K_p^T \Omega_i^2 \end{pmatrix} \quad (7)$$

  Where K_p^T is the thrust coefficient of the motor and Ω_i is the rotational speed of the motor. The thrust coefficient of the motor was identified by bench test of the motor-propeller system.
- F_a^{wb} : Aerodynamic forces produced by the vehicle in the earth frame:

$$F_a^{wb} = R_{eb} R_{bw} \begin{pmatrix} -D^{wb} \\ Y^{wb} \\ -L^{wb} \end{pmatrix} \quad (8)$$

  Where D_{wb}, Y_{wb} and L_{wb} represent the simplified forces acting on the vehicle in the wind reference frame and can be expressed as follows [6]:

$$\begin{pmatrix} D^{wb} \\ Y^{wb} \\ L^{wb} \end{pmatrix} = Q \begin{pmatrix} C_{D0} + k_{cd}(C_{L0} + C_{L\alpha}\alpha)^2 \\ C_{Y\beta}\beta \\ C_{L0} + C_{L\alpha}\alpha \end{pmatrix} \quad (9)$$

$$Q = \frac{1}{2}\rho S V_{tot}^2$$

  Where ρ is the air density, S is the wing surface and V_{tot} is the airspeed.

- M_a^{wb} : Aerodynamic moments produced by the vehicle in the body frame:

$$M_a^{wb} = \begin{pmatrix} M_L^{wb} \\ M_M^{wb} \\ M_N^{wb} \end{pmatrix} = \\ = Q \begin{pmatrix} \bar{b}(C_{l0} + C_{l\beta}\beta + \frac{\bar{b}}{2V_{tot}}(C_{lp}p + C_{lr}r)) \\ \bar{c}(C_{m0} + C_{m\alpha}\alpha) \\ \bar{b}(C_{np}\frac{\bar{b}}{2Vtot}p + C_{nr}\frac{\bar{b}}{2V_{tot}}r) \end{pmatrix} \tag{10}$$

where M_L^{wb}, M_M^{wb} and M_N^{wb} represent respectively the vehicle roll, pitch and yaw moment induced by the wind [6]. The coefficients for the aerodynamic equations can be identified through test flight, CFD analysis or from geometrical vehicle properties [8]. Note that some coefficients are not present in the expression and considered negligible, because the vehicle is tailless and the CG is located very close to the quarter chord point [8].

- M_p^T : Torque generated by the rotors due to the propeller thrust:

$$M_p^T = \sum_{i=1}^{N} \left(R_{bp}^i \cdot \begin{bmatrix} 0 \\ 0 \\ -K_p^T \Omega_i^2 \end{bmatrix} \right) \times \begin{pmatrix} l_x^i & l_y^i & l_z^i \end{pmatrix} \tag{11}$$

Where (l_x^i, l_y^i, l_z^i) are the coordinate of the i-th rotor in the body reference frame.

- M_p^D : Torque generated by the rotors due to the propeller drag:

$$M_p^D = \sum_{i=1}^{N} -R_{bp}^i \begin{pmatrix} 0 \\ 0 \\ K_p^M \Omega_i^2 \end{pmatrix} (-1)^i \tag{12}$$

Where K_p^M is the torque coefficient of the motor and can be evaluated in the same way as K_p^T.

- M_p^I : Torque generated by the propeller inertia due to the propeller rate change:

$$M_p^I = \sum_{i=1}^{N} -J_p R_{bp}^i \begin{pmatrix} 0 \\ 0 \\ \dot{\Omega}_i \end{pmatrix} (-1)^i \tag{13}$$

- M_r^p : Torque generated by the rotor precession term due to the tilting rotation:

$$M_r^p = \sum_{i=1}^{N} R_{bp}^i \begin{pmatrix} 0 \\ 0 \\ J_p \Omega_i \end{pmatrix} \times \begin{pmatrix} \dot{g}_i \\ \dot{b}_i \\ 0 \end{pmatrix} (-1)^i \tag{14}$$

- M_r^{tilt} : Torque generated by the rotor inertial term due to the tilting rotation:

$$M_r^{tilt} = \sum_{i=1}^{N} R_{bp}^i \begin{pmatrix} \ddot{g}_i I_{xx_i}^{tilt} \\ \ddot{b}_i I_{yy_i}^{tilt} \\ 0 \end{pmatrix} (-1)^i \tag{15}$$

- M_p^t : Inertial term of the rotor due to the vehicle rates

$$M_p^t = \sum_{i=1}^{N} -\omega \times \left(R_{bp}^i I_p \begin{pmatrix} 0 \\ 0 \\ \Omega_i \end{pmatrix} (-1)^i \right) \tag{16}$$

Where I_p is the propeller inertia in the propeller frame, in this case simplified to:

$$I_p = \begin{pmatrix} 0 & 0 & 0 \\ 0 & 0 & 0 \\ 0 & 0 & J_p \end{pmatrix}$$

C. Servo load expression

It is possible to calculate the effective torque load on the servomotors. The total load on the servos is the addition of the rotor precession term (in propeller frame) and the inertial term related to the tilting moment of inertia. For every rotor, the servo load is thus given by:

$$S_{az}^i = G_r^a(-J_r \Omega_i \dot{b}_i(-1^i) + \ddot{g} I_{xx_i}^{tilt}) \\ S_{el}^i = G_r^e(-J_r \Omega_i \dot{g}_i(-1^i) + \ddot{b} I_{yy_i}^{tilt}) \tag{17}$$

Where S_{az}^i and S_{el}^i are respectively the torque on the azimuth and elevation servo of the i-th rotor while G_r^a and G_r^e are the azimuth and elevation gear ratio between the servo and the rotating mechanism. Notice that in that expression, the torque related to the mass of the tilting system, as well as the damping term due to the propeller aerodynamic effects are not considered.

IV. Actuator Model Identification

To complete the vehicle modeling, the actuators were identified, modeled and mapped through several tests. Two types of actuators are present in the UAV. The first type of actuator is the propulsion system whose dynamics are driven mainly by the propeller-motor interaction. Specifically, a T-motor AT-2312 1150kV was used, coupled with a nylon 9x4.7 propeller, a Turnigy MultiStar 30A BLHeli-S Electronic Speed Controller(ESC) and a 3S 5000mAh 25C Turnigy LiPo battery.

The second type of actuator is the servo, found in the rotor tilt mechanism. This system is driven by two SAVOX 1232MG servos and its dynamics are related to the tilting system inertia, to the rotor precession term and to the propeller damping.

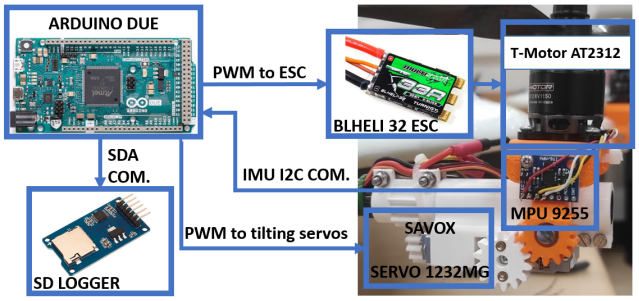

Fig. 6: Scheme of the testing setup for the tilting mechanism dynamics acquisition.

A. Experimental setup

To analyze the motor dynamics characteristics, the HOBBYWING RC Model Brushless RPM Sensor AC683 was used. This sensor is directly connected on two motor poles and generates a PWM signal associated to the rotational speed of the motor. For the motor step test, an arduino DUE was used to generate the Pulse Width Modulation (PWM) input to the ESC and to simultaneously monitor the RPM sensor output.

Concerning the tilting rotor dynamics, the most straightforward way to monitor the tilting angles would be through the servomotor feedback. However, the servos do not provide any telemetry information and therefore an MPU9255 Inertial Measurement Unit (IMU) rigidly attached to the tilting mechanism was used to record the tilting orientation. An arduino DUE was used to send commands to the actuators, to monitor the IMU and to log the data onto an external SD card. A scheme of the testing setup is visible in Fig.6.

B. Results

For the motor dynamics identification, few step input were fed to the ESC. Fig. 7 shows the evolution of the fed PWM value, together with the recorded motor rotational speed.

Similar step inputs were fed to the azimuth and elevation servos of the tilting system[2]. In Fig. 8 the elevation and azimuth tilting angle response to a 60 degree step is shown while the motor (with propeller) was running. To evaluate the effect of the turning propeller on the tilting dynamics, the experiment was performed with the motor running at 25% and 100% thrust level. In Fig. 9 the same tilting angle dynamics is reported for a 70 degrees step input in the elevation axis. An interesting observation coming from the tilting test is the presence of the gyroscopic precession term of the rotor tilting. These dynamics are visible in the form of azimuth angle perturbation in the tilting elevation test and vice-versa. The effect increases with increasing throttle value, as analyzed in the servo load expression presented in Equation 17.

[2]https://youtu.be/QNZSxoJ1Gto

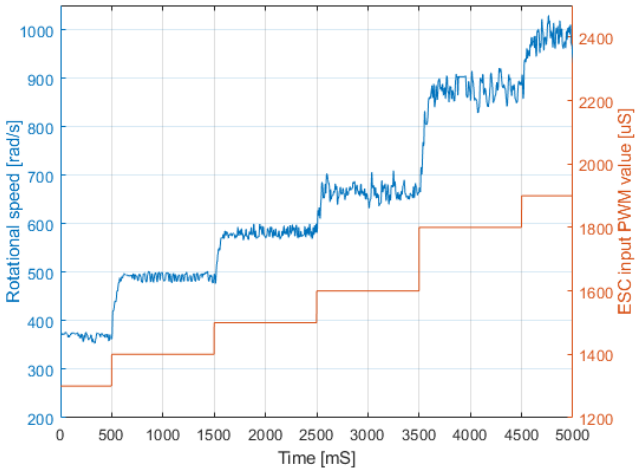

Fig. 7: Test for the motor dynamics characterization. The red curve shows the PWM value fed to the ESC while the blue curve shows the rotational speed evolution of the motor.

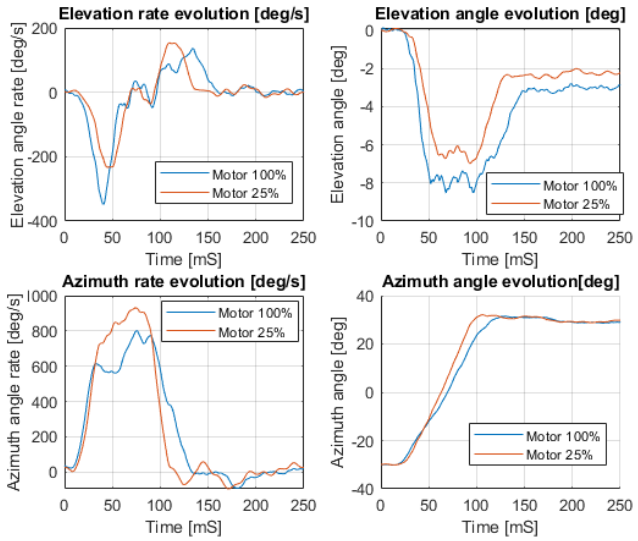

Fig. 8: Tilting angles and rate evolution to an azimuth step response of around 60 degrees at different motor power level.

The motor and servomotor dynamics were modeled as first order system with delay:

$$H(s) = e^{-\tau_d \cdot s} \cdot \frac{\omega_c}{s + \omega_c} \tag{18}$$

where τ_d is the actuator delay and ω_c is the actuator cutting frequency. The actuators dynamics characteristics identified through the actuator tests for the servomotors and the motor dynamics are summarized in Table IV. Even though the servomotors used are the same, the azimuth and elevator dynamics are slightly different due to the different gear ratio used.

V. Wind Rejection Capabilities and Simulation

In this Section, using the mathematical model and the actuator dynamics as a reference, a set of simulations are

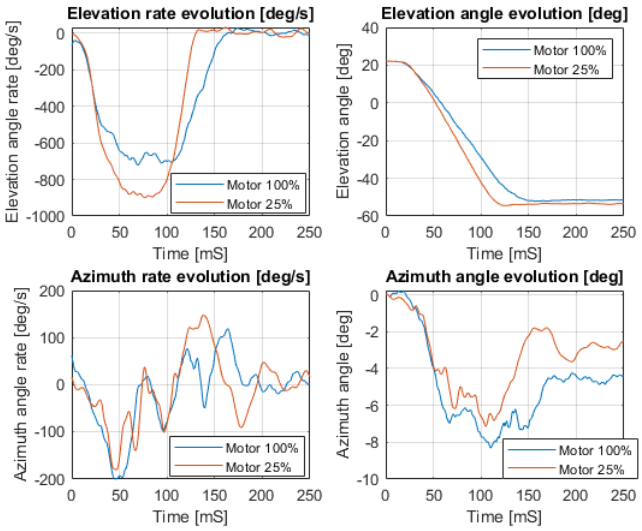

Fig. 9: Tilting angles and rate evolution to an elevation step response of around 60 degrees at different motor power level.

Motor delay τ_d^m	2 mS.
Elevation servo delay τ_d^e	15 mS.
Azimuth servo delay τ_d^a	15 mS.
Motor dynamics ω_c^m	30 rad/s
Azimuth servo dynamics ω_c^a	30.7 rad/s
Elevation servo dynamics ω_c^e	26.2 rad/s

TABLE IV: Actuator dynamics characteristics

performed to characterize and compare the performance of the presented over-actuated quad-plane with a conventional quad-plane design. Firstly, from the equations of motion established in Section 3, it is possible to characterize the system of equations at equilibrium for a stationary, symmetric flight condition ($\beta = 0$) for both the proposed and the conventional quad-plane in the hovering configuration. In Eq. 19 and Eq. 20, the system of equations at equilibrium for the conventional and for the over-actuated quad-plane vehicle are shown respectively.

$$\begin{cases} (F_1+F_2+F_3+F_4)sin(\theta) = -D_{wb} \\ (F_1+F_2+F_3+F_4)cos(\theta) = mg - L_{wb} \\ (F_3+F_4)l_3 - (F_1+F_2)l_4 = M_{wb} \\ F_1 = F_2 \\ F_3 = F_4 \end{cases} \tag{19}$$

$$\begin{cases} (F_1+F_2+F_3+F_4)sin(b_{tot}+\theta) = -D_{wb} \\ (F_1+F_2+F_3+F_4)cos(b_{tot}+\theta) = mg - L_{wb} \\ (F_3+F_4)l_3cos(b_{tot}) - (F_1+F_2)l_4cos(b_{tot}) = M_{wb} \\ F_1 = F_2 \\ F_3 = F_4 \end{cases} \tag{20}$$

Here D_{wb} and L_{wb} are already expressed in the earth reference frame and F_i represents the motor thrust in the propeller reference frame.

From these equations it is possible to determine the equilibrium pitch angle θ_{eq} (in conventional quad-plane configuration) and elevator tilting angle b_{eq} (in the over-actuated quad-plane configuration, supposing $\theta = 0$) to counteract a specific constant wind speed without losing altitude.

Cl_α	4.2 rad^{-1}
Cl_0	-0.05
Cm_α	-0.58 rad^{-1}
Cm_0	0.002
k_{cd}	0.08
C_{D0}	0.55

TABLE V: Aerodynamic coefficients for the vehicle

The lift and moment coefficients for the aerodynamics used in the simulations are derived from the XFLR5 analysis, the zero-lift drag coefficient C_{D0} is obtained from the wind tunnel test and the k_{cd} coefficient is calculated as follows: $k_{cd} = \frac{1}{\pi A_r e}$ [8]. An overview of the aerodynamic coefficients used for the simulation are reported in Table V.

A. Simulation setup and results

A diagram of the control system used to simulate the conventional quad-plane and the over-actuated quad-plane vehicle is reported respectively in Fig. 10 and Fig. 11. For clean comparison, the same altitude and attitude PID controller were used for the two vehicle configurations. The PID gains used for the altitude are $P = 600\frac{rad/s}{rad}$, $I = 100\frac{rad/s}{rad \cdot s}$ and $D = 500\frac{rad/s}{rad/s}$, while the PID gains used for the theta controller are $P = 390\frac{rad/s}{rad}$, $I = 500\frac{rad/s}{rad \cdot s}$ and $D = 110\frac{rad/s}{rad/s}$. The PID coefficients for the theta controller were tuned using the open loop bode plot of the equivalent linear system as a main reference, ensuring a final open loop dynamics of 12.8 rad/s and a phase margin of 30 deg. The saturation points for the PID controllers on the desired motor rotational speed are $[-600, 600]$ rad/s for the theta controller and $[-500, 500]$ rad/s for the altitude controller.

The equilibrium point for theta (θ_{eq}) and the elevator tilting angle (b_{eq}) are a function of the wind speed and are computed using Eq. 19 and Eq. 20 respectively.

In Fig. 12, the simulated acceleration response with a frontal step wind of 5 m/s is shown for both the conventional and the over-actuated quad-plane. Similarly, Fig. 13 shows an acceleration test performed in absence of wind. During the tests, the conventional and over-actuated vehicles are requested to reach the previously determined θ_{eq} and b_{eq} condition. Considering the acceleration test in absence of wind, the acceleration peak is reached at 0.22 seconds on the over-actuated vehicle and at 0.75 seconds on the conventional quad-plane. With these simulations we can therefore conclude that tilting the rotors instead of the whole vehicle leads to a much faster acceleration response and a more effective wind gust rejection capability.

VI. Flight Test Results

In this section, the results of the wind tunnel experiments are analyzed. The main focus of the test flights was to validate the simulated response and to extend the vehicle

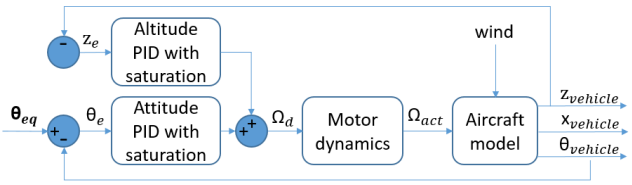

Fig. 10: Control scheme for the conventional quad-plane configuration.

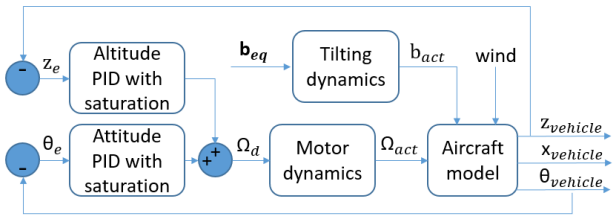

Fig. 11: Control scheme for the over-actuated quad-plane vehicle. b is the overall elevation tilting angle of the rotors, assumed to be the same for all the four rotors.

gust response also to the lateral gust scenario. The wind tunnel experiments were also used to estimate the zero-lift drag coefficient of the vehicle.

A. Experimental setup

For the wind tunnel experiment, the Paparazzi open-source software[3] was used, running on a Holybro Pixhawk 4 flight computer. In order to simulate a discrete wind step response in the wind tunnel, the vehicle was introduced into the flow region from the bottom, to minimize the attitude change during the transition phase. For a better understanding of the wind tunnel testing setup, a picture of the wind tunnel flight test experiment is shown in Fig. 14.

For the over-actuated quad-plane setup, an Incremental Non-linear Dynamic Inversion (INDI) controller [9] was used to control the attitude of the vehicle using only the motors, the tilting system was controlled using a PD control with feedback of the vehicle position.

For the conventional quad-plane setup, the tilting angle g_i and b_i were set to zero for all the rotors. The attitude was controlled with the same INDI controller as in the over-actuated configuration. In that case, the position of the vehicle was controlled via an outer PD loop through attitude changes. For both the conventional and over-actuated quad-plane configuration, the yaw was controlled by means of differential azimuth tilting angle.

B. Test results

Frontal wind gust and lateral wind gust response experiments were performed at a wind speed of 5 m/s for both the over-actuated and the conventional quad-plane configuration[4]. Figure 15 shows the results of the frontal wind gust experiment. It can be observed that when the tilting system is active, the vehicle is able to hold its current position with a maximum displacement of around 20 cm and a maximum pitch perturbation of 5 degrees. On the other hand, the conventional quad-plane vehicle reached an equilibrium pitch angle of around 10 degrees with a maximum displacement of more than 1.4 meters.

Similar behavior can be observed for the lateral wind gust flight test, displayed in Fig. 16. Interestingly, during the lateral gust flight tests both the over-actuated and conventional quad-plane vehicle suffered from low frequency oscillations in the roll dynamics. This may be related to the lower roll authority of the vehicle with the present motor disposition. Saturation of the front right motor is observed during the maneuver.

Finally, considering the frontal gust tests of the conventional quad-plane, it is possible to identify an equilibrium pitch angle that the vehicle reaches to react to the wind gust. By knowing the wind speed, and observing stationary condition for the flight test, we can replace the equilibrium theta and the wind speed in equation (19). Substituting the lift and moment coefficients with the XFLR5 analysis result and the induced drag coefficient with $k_{cd} = \frac{1}{\pi A_r e}$, it is possible to estimate the vehicle zero-lift drag coefficient C_{D0}. The result of the fitted drag coefficient for the vehicle is equal to $C_{D0} = 0.55$. This completes the longitudinal aerodynamic model identification of the UAV.

VII. Conclusions

In this paper a novel quad-plane design capable of full 6DOF control was presented and modeled. Through wind tunnel experiments and simulations, the effectiveness of the rotor tilting strategy to handle rapid and unpredictable wind gusts and to achieve rapid linear accelerations in any direction was proved. In particular, considering the simulation results, the over-actuated quad-plane is 3.4 times more responsive than the conventional quad-plane in achieving linear acceleration. The spot hover capability in gusty environment was tested through a wind tunnel experiment simulating a frontal 5 m/s gust, leading to a displacement of just 0.2 meters for the over-actuated vehicle compared to the 1.4 meters of the conventional quad-plane. Similar behavior was observed in the lateral gust experiment. Dual-axis tilting rotors are therefore a good option to enhance the wind rejection capabilities of a conventional quad-plane vehicle.

Future research will focus on the development of a tailored control system for the UAV, able to homogeneously control the vehicle in both the forward and the hovering flight phase. Finally, flight performance of the vehicle will be tested at different unconventional attitude conditions.

Acknowledgment

This work was carried out within the Unmanned Valley Project. The authors would like to thanks the "Europees

[3]https://wiki.paparazziuav.org/wiki/Main_Page
[4]https://youtu.be/xCXokABB4B0

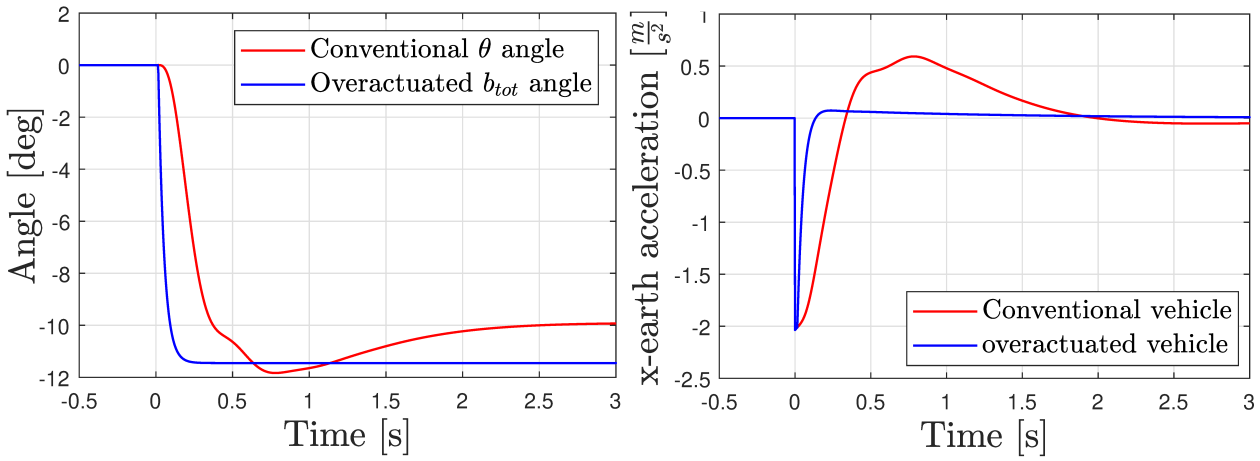

Fig. 12: Simulation result to a 5 m/s frontal wind step. The blue curve represent the over-actuated vehicle while the red curve represent the conventional quad-plane.

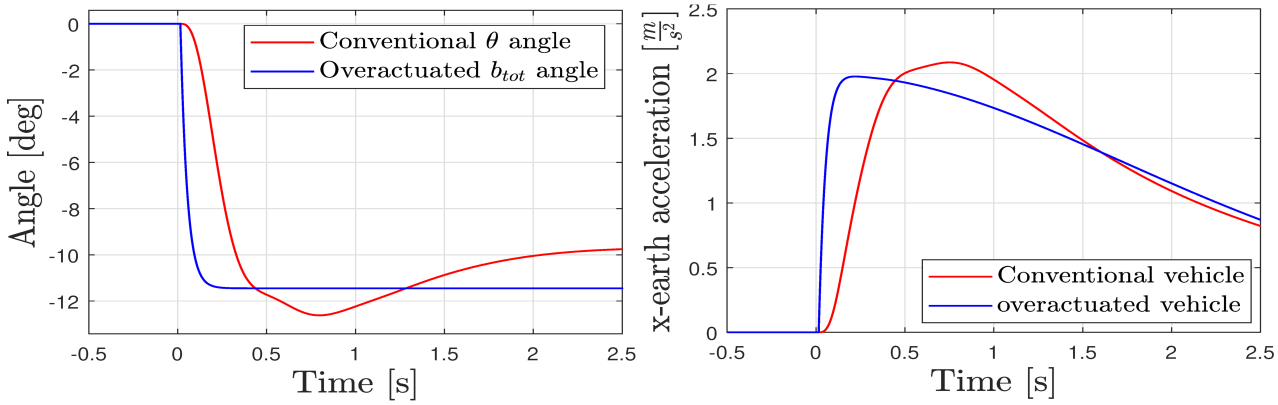

Fig. 13: Simulation result to a required forward acceleration without wind. The blue curve represent the over-actuated vehicle while the red curve represent the conventional quad-plane.

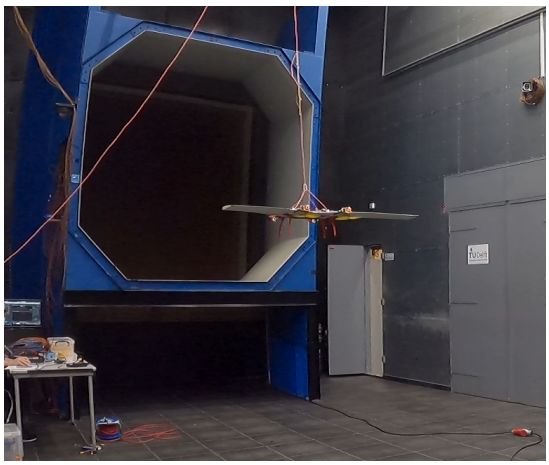

Fig. 14: Picture of the wind tunnel test experiment.

Fonds voor Regionale Ontwikkeling(EFRO)" who is founding the Unmanned Valley project under grant code KvW-00168 for the South-Holland region.

REFERENCES

[1] Alwin R. Wang: *Conceptual Design of a QuadPlane Hybrid Unmanned Aerial Vehicle.* AIAA Student Conference Region VII-AU , 2017. doi:10.13140/RG.2.2.23090.84163

[2] Gerardo Ramon Flores, Juan Escareño, Rogelio Lozano, Sergio Salazar: *Quad-Tilting Rotor Convertible MAV: Modeling and Real-Time Hover Flight Control.* Intelligent Robot Systems , 2012. doi:10.1007/s10846-011-9589-x

[3] AN Chen, Zhang DaiBing, Zhang JiYang, Li TengXiang: *A New structural configuration of tilting rotor unmanned aerial vehicle modeling.* 35th Chinese Control Conference, 2016. doi:10.1109/ChiCC.2016.7553680

[4] Hang Zhang, Bifeng Song, Haifeng Wang and Jianlin Xuan: *A method for evaluating the wind disturbance rejection capability of a hybrid UAV in the quadrotor mode.* International Journal of Micro Air Vehicles, 2019. doi:10.1177/1756829319869647

[5] Ali Bin Junaid, Alejandro D.D.C. Sanchez, Javier B. Bosch, Nikolaos Vitzilaios and Yahya Zweiri: *Design and Implementation of a Dual-Axis Tilting Quadcopter.* Journal of robotics, 2018. doi:10.3390/robotics7040065

[6] Vladislav Klein, Eugene A Morelli: *AIRCRAFT SYSTEM IDENTIFICATION : THEORY AND PRACTICE.* Blackurg,Virginia,2006, Chapter 3.

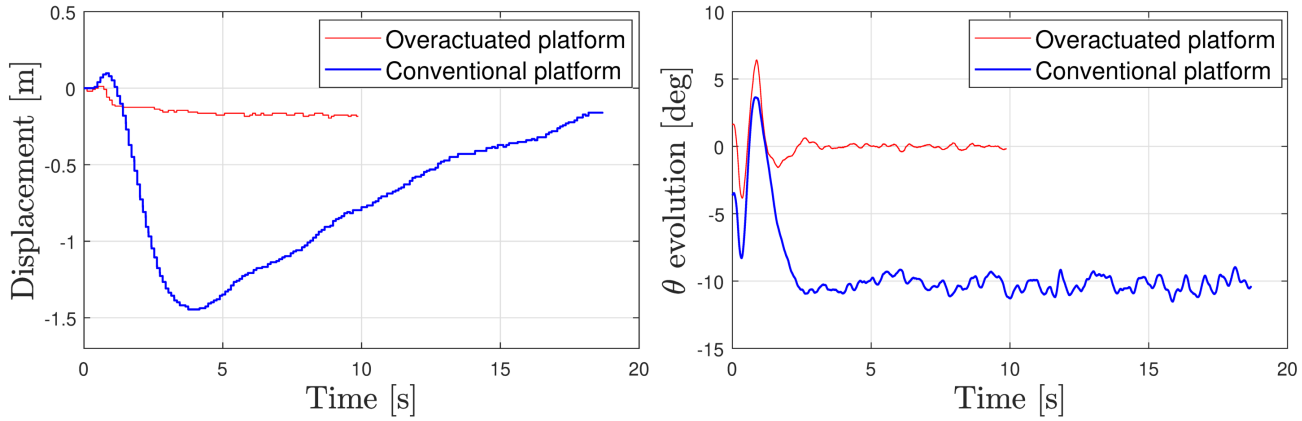

Fig. 15: Position displacement and pitch evolution to a 5 m/s frontal wind gust flight test experiment performed in the wind tunnel. The blue curve represent the over-actuated vehicle response while the red curve represent the conventional quad-plane response.

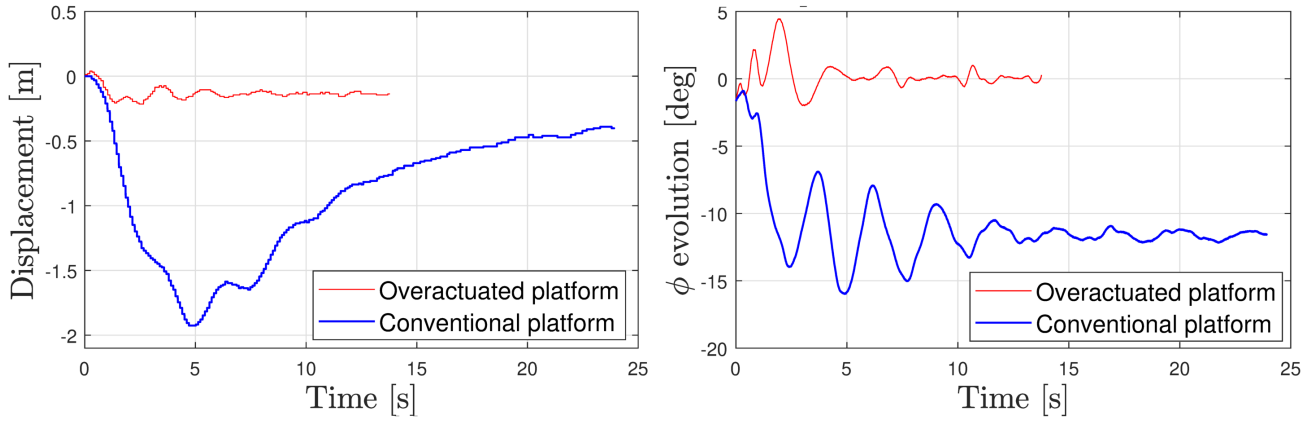

Fig. 16: Position displacement and roll evolution to a 5 m/s lateral wind gust flight test experiment performed in the wind tunnel. The blue curve represent the over-actuated vehicle response while the red curve represent the conventional quad-plane response.

[7] Alexandra Moutinho, Estanislao Mateos and Filipe Cunha: *The tilt-quadrodot:concept, modeling and identification.* IEEE International Conference on Autonomous Robot Systems and Competitions, 2015. doi:10.1109/ICARSC.2015.38

[8] Frederick O. Smetana, Delbert C. Summey and W. Donald Johnson *RIDING AND HANDLING QUALITIES OF LIGHT AIRCRAFT - A REVIEW AND ANALYSIS.* National aeronautics and space administration, Washinton DC, March 1972

[9] Ewoud Jan Jacob Smeur, P. Chu and Guido de Croon: *Adaptive Incremental Nonlinear Dynamic Inversion for Attitude Control of Micro Air Vehicles.* Journal of Guidance, Control, and Dynamics, 2015. doi:10.2514/1.G001490

[10] Markus Ryll, Heinrich H Bülthoff and Paolo Robuffo Giordano: *Modeling and control of a quadrotor UAV with tilting propellers.* Robotics and Automation (ICRA), 2012. doi:10.2514/1.G001490

[11] Xinhua Wang and Lilong Cai: *Mathematical modeling and control of a tilt-rotor aircraft.* Aerospace Science and Technology. Volume 47, December 2015, Pages 473-492. doi:10.1016/j.ast.2015.10.012

[12] Riccardo Falconi and Claudio Melchiorri: *Dynamic Model and Control of an Over-actuated Quadrotor UAV.* 10th IFAC Symposium on Robot Control International Federation of Automatic Control, 2012. doi:10.3182/20120905-3-HR-2030.00031

[13] Sujit Rajappa, Markus Ryll, Heinrich H. Bülthoff and Antonio Franchi: *Modeling, control and design optimization for a fully-actuated hexarotor aerial vehicle with tilted propellers.* IEEE International Conference on Robotics and Automation 2015. doi:10.1109/ICRA.2015.7139759

[14] Muhammad Umer, Syed Mohsin Abbas Kazmi, Syed M. Hassan Askari and Iftikhar Ahmad Rana: *Design and Modeling of VTOL Tri Tilt-rotor Aircraft.* 15th International Conference on Smart Cities: Improving Quality of Life Using ICT & IoT (HONET-ICT), 2018. doi:10.1109/HONET.2018.8551474

[15] Fatih Şenkul and Erdinç Altuğ: *Modeling and control of a novel tilt — Roll rotor quadrotor UAV.* 15th International International Conference on Unmanned Aircraft Systems (ICUAS), 2013. doi:10.1109/ICUAS.2013.6564796

[16] Mahmoud Elfeky, M. Elshafei, A. A. Saif and M. F. Al-Malki: *Quadrotor helicopter with tilting rotors: Modeling and simulation.* 2013 World Congress on Computer and Information Technology (WCCIT), 2013, pp. 1-5. doi:10.1109/WCCIT.2013.6618768